WILEY The International Journal of **Medical Robotics** and **Computer Assisted Surgery**

ORIGINAL ARTICLE

ConoSurf: Open-source 3D scanning system based on a conoscopic holography device for acquiring surgical surfaces

Mikael Brudfors[1] | Verónica García-Vázquez[2] | Begoña Sesé-Lucio[2] | Eugenio Marinetto[2] | Manuel Desco[1,2,3] | Javier Pascau[1,2,3]

[1] Departamento de Bioingeniería e Ingeniería Aeroespacial, Universidad Carlos III de Madrid, Madrid, Spain

[2] Instituto de Investigación Sanitaria Gregorio Marañón (IiSGM), Madrid, Spain

[3] Centro de Investigación Biomédica en Red de Salud Mental (CIBERSAM), Madrid, Spain

Correspondence
Javier Pascau, Departamento de Bioingeniería e Ingeniería Aeroespacial, Universidad Carlos III de Madrid, Avda. de la Universidad, 30. 28911 Leganés, Madrid. Spain.
Email: javier.pascau@uc3m.es

Abstract

Background   A difficulty in computer-assisted interventions is acquiring the patient's anatomy intraoperatively. Standard modalities have several limitations: low image quality (ultrasound), radiation exposure (computed tomography) or high costs (magnetic resonance imaging). An alternative approach uses a tracked pointer; however, the pointer causes tissue deformation and requires sterilizing. Recent proposals, utilizing a tracked conoscopic holography device, have shown promising results without the previously mentioned drawbacks.

Methods   We have developed an open-source software system that enables real-time surface scanning using a conoscopic holography device and a wide variety of tracking systems, integrated into pre-existing and well-supported software solutions.

Results   The mean target registration error of point measurements was 1.46 mm. For a quick guidance scan, surface reconstruction improved the surface registration error compared with point-set registration.

Conclusions   We have presented a system enabling real-time surface scanning using a tracked conoscopic holography device. Results show that it can be useful for acquiring the patient's anatomy during surgery.

1 | INTRODUCTION

During computer-assisted interventions (CAI), localization information from tracking systems is commonly combined with imaging to provide accurate guidance. In soft-tissue CAI, a major difficulty is the acquisition of the patient's anatomy during surgery. If the anatomy can be acquired in a fast and reliable way it can then be used for registration of preprocedural information such as images and/or models.[1] Having the preprocedural information added to the patient frame could then add valuable guidance to the surgeon, including visualization of internal features before and during incisions.[2] Furthermore, it also enables surgical tools, such as cauteries and needles, to be accurately guided to the desired targets.[3]

Several standard modalities can be used for intraoperative patient localization, including ultrasound (US), intraoperative computed tomography (CT) and interventional magnetic resonance imaging

(iMRI).[4–6] However, these modalities have several drawbacks when used in the intraoperative domain and may not be well-suited for real-time image acquisition due to low image quality, ionizing radiation exposure, incompatibility with traditional instrumentation and/or high costs. Another approach uses surface points collected from the patient with an electromagnetically or optically tracked pointer. These surface points can then be registered to surface features identified in preoperative images. One source of error of this approach is the tissue deformation that occurs when the pointer is moved along the tissue surface.[7] In addition, the pointer device must be sterilized in advance and may be awkward to introduce into surgical cavities during procedures.

Laser range scanners (LRS) overcome the pointer limitations in terms of sterility, possible deformations to tissues and surface registration error (SRE),[7] and have been used for image-guided procedures.[8] However, Simpson et al[9] showed that a conoscopic holography device

could obtain a lower SRE than a LRS while additionally being able to acquire surfaces inside surgical cavities (which may not be possible with a LRS). Furthermore, Lathrop et al[10] reported the use of the tracked ConoProbe as a promising surface acquisition device in the operating room and, in a recent paper,[11] the ConoProbe was used to digitize the interior of the resection cavity during eight brain tumour resection surgeries, and these surfaces were then compared against model prediction results of tumour locations.

The ability of the ConoProbe to scan surgical cavities motivated our interest in this device, as we would like to improve the dose estimation in intraoperative electron radiation therapy (IOERT) procedures. IOERT involves irradiation of a tumour volume or a post-resected tumour bed with an electron beam during surgery. In previous work,[12] we have presented an initial study of CT imaging during the procedure, but the need for a CT scanner during surgery is a major drawback. For intraoperative radiotherapy, estimating the dose distribution is a challenging task, due to irregular treatment surfaces and biologic fluid accumulation.[13,14] Intraoperative surface scanning could provide information on the tumour bed to be irradiated which could be used to update the dose estimation according to the actual patient's anatomy. In addition, the ConoProbe could also act as a pointing device during an image-guided scenario.

Although previous studies have presented the advantages of the use of ConoProbe in image-guided surgery, these contributions are not available as open-source software, limiting the capacity of other researchers to evaluate the possible use of this device for their specific applications. Therefore, in this paper we present an open-source solution, which we call ConoSurf that enables the use of the ConoProbe in an image-guided therapy workflow, facilitating further contributions from the research community. ConoSurf integrates with the 3D Slicer software,[15] which offers advanced medical image processing and interaction capabilities, and the Plus Toolkit,[16] which facilitates hardware integration. We identified several goals to be addressed by our solution, which were not available in previous work on the application of the ConoProbe in image-guided therapy:

- Ability to modify the tracking system used to acquire the position of the ConoProbe by using the Plus Toolkit.
- Real-time visualization of the acquired points during the scanning process with color-coded positions to facilitate 3D visualization, allowing revisiting of surface areas with lower sampling densities.
- Possibility to store all the acquired data in order to modify the preprocessing parameters offline, evaluating the effect on the resulting dataset.
- Surface reconstruction from the complex set of unorganized points obtained from the scanning process resulting in a smooth mesh.

The proposed ConoSurf system is tested on several complex phantoms: a multi-step phantom to assess the system's depth measuring capability; cavities with and without fluids, in order to evaluate the system's ability to scan a more complex object and to assess the system's behaviour when working with fluids; and finally a breast phantom, to simulate a quick surface acquisition during an image-guided intervention. Full documentation and source code of our project can be found at http://hggm-lim.github.io/ConoSurf/.

2 | MATERIALS AND METHODS

There exist several challenges in creating a 3D scanning system using a conoscopic holography sensor. On the hardware side, we need to decide on a tracking system in order to enable acquisition of spatial surface measurements; provide a way of defining both spatial and temporal calibration between the sensor and the tracker; and synchronize the two data streams. On the software side, we need to design an intuitive user interface; allow for saving, filtering and post-processing of the recorded points; and implement a fast and robust method for surface reconstruction from the unorganized points. The remainder of this section will describe how these challenges were overcome: the hardware parts which the system contains (section 'System components'), the integration of this hardware into a system for 3D scanning (section 'System integration') and the evaluation of the 3D scanning system (section 'System evaluation'). An overview of the system implementation is shown in Figure 1.

3 | SYSTEM COMPONENTS

3.1 | Conoscopic holography device

Conoscopic holography is a low-cost, commercially available technology based on polarized light interference. The conoscopic holography sensor used in this paper is called ConoProbe (ConoProbe Mark 10 [Optimet Metrology Ltd, Israel]) and is shown in Figure 2. The ConoProbe can acquire measurements with a frequency of up to 9 kHz and can be used with different lenses depending on the distance range and precision needed for the application. In this work we use a 250 mm lens with a measurement range from 155 to 335 mm. This lens was chosen in order to increase the distance of the ConoProbe from the patient, because the device cannot be sterilized. Furthermore, it was also the lens used in previous studies involving the ConoProbe and CAI.[10,17] The lens is assigned the coordinate frame L. The stated accuracy of the measurement of the ConoProbe lens is 80 μm, and the precision is 35 μm. The laser in the ConoProbe is a class II red diode laser with a wavelength of 655 nm and a maximum output power of 1 mW. The laser spot size, specified by the manufacturer, is 107 μm.

3.2 | Multi-camera optical tracking system

In order to enable acquisition of a spatial surface measurement, the ConoProbe itself has to be located by means of an additional localization sensor. We selected an optical tracking system called OptiTrack (NaturalPoint Inc., OR, USA) for this purpose. Unlike most optical tracking systems used in image-guided surgery (utilizing a fairly small number of cameras), OptiTrack is a multi-camera system. This results in improved practical use in complex clinical scenarios, where the required line-of-sight between the tracked objects and the cameras is easily obstructed.[18] A potential disadvantage of this type of tracking system is that it requires a camera calibration with respect to both extrinsic (physical position and orientation) and intrinsic parameters (focal length and lens distortion). Three synchronized cameras (OptiTrack FLEX:V100R2, NaturalPoint Inc.), with a resolution of 640 × 480 pixels (VGA) and maximum frame rate of 100 FPS were placed around the scenario. This multi-camera approach covers a large
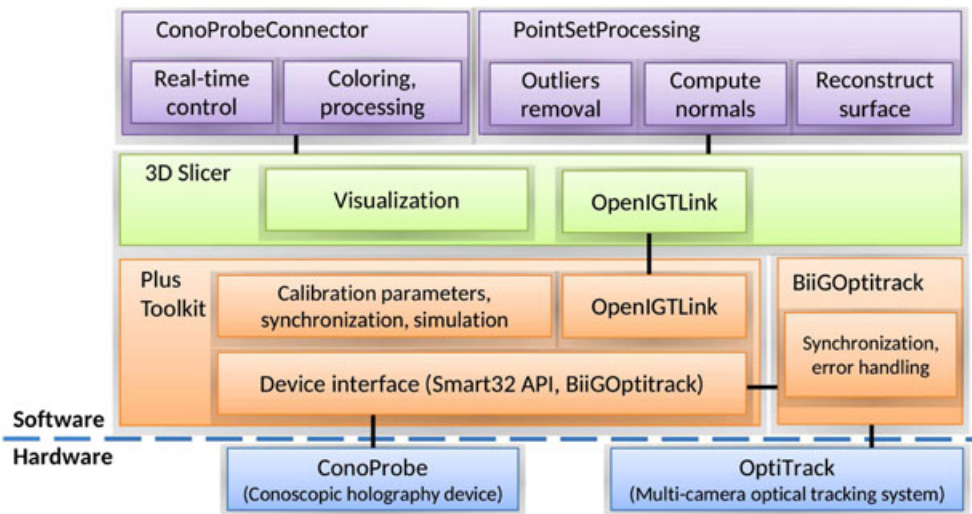
FIGURE 1 The implementation overview of the ConoSurf 3D scanning system. The data from the ConoProbe and the Optitrack is obtained through the Plus Toolkit and the BiiGOptitrack library. This data is then transmitted, via OpenIGTLink, to 3D Slicer where the modules are made available

FIGURE 2 The ConoProbe conoscopic holography device with attached rigid body

working volume, thus making it well suited for point acquisition in the operating room, where it is often necessary to capture points from multiple sides of an object. A rigid body, which is assigned the coordinate frame C, was fixed onto the sensor housing of the ConoProbe, parallel to one wall of the housing (Figure 2). The transform T, from the tracker's reference coordinate frame to C, provides position and orientation information. The rigid body is composed of four retro-reflective optical markers. The optical tracking system's extrinsic and intrinsic parameters were calibrated using a three-marker OptiWand (NaturalPoint Inc.) and the calibration algorithm part of the Tracking Tools software (NaturalPoint Inc.).

4 | SYSTEM INTEGRATION

4.1 | Temporal calibration

Based on the maximum frame rate of the optical tracking system, a measurement frequency of 100 Hz is chosen for the ConoProbe. In

order to determine the time offset (τ) between the two data streams, a temporal calibration is necessary. This calibration procedure is similar to the one followed in US-guided surgery,[19] in which principal component analysis (PCA) is applied to the data streams and afterwards their first principal components are cross-correlated in order to obtain the time offset. In our case, PCA is applied only to the position data since the measurement data have one degree of freedom.

4.2 | Spatial calibration

In order to establish the spatial relationship between the tracked rigid body and the ConoProbe measurements, a spatial calibration is necessary. In this work, the calibration technique closely follows the technique used by Burgner et al.[17] By defining the laser beam direction as $\widehat{d}$ (which corresponds to one axis in the lens frame L), the measured distance as d_i (with respect to the origin of L), and the translational offset with respect to the frame C as l. A measured point p_i can be expressed in the coordinate frame of the optical tracker as $p_i = T_i\left(l + d_i\widehat{d}\right)$, where T_i is the transform from the tracker coordinate frame to frame C. By acquiring ground-truth (GT) measurements p_i', the vectors l and $\widehat{d}$ can be determined by a least squares fitting between the GT points and the points obtained with the tracked ConoProbe (that is, by minimizing $\sum_{i=1}^{N}\left\|p_i - p_i'\right\|_2^2$).

4.3 | Plus Toolkit integration

In order to acquire the distance measurements from the ConoProbe, and the pose information from the OptiTrack system, a dedicated hardware interface was developed. Natural Point provides an application programming interface (API) in order to control the multi-camera optical tracking system. However, controlling the tracker hardware directly using the API is not suitable for clinical applications where robust error handling is critical for proper system error recovery. Hence, we developed the BiiGOptitrack library* to interface with the

---

*BiiGOptitrack library, http://github.com/HGGM-LIM/BiiGOptitrack

tracker. BiiGOptitrack follows the tracking interface standard defined by the OpenIGTLink protocol,[20] allowing for connection to the tracker, tracked tools management and safe recovery from errors during tracking acquisition. The most interesting advantage of BiiGOptitrack is the threading-based tracking that allows for real-time data acquisition while ensuring tracked tools are inside the field of view of the cameras, all markers forming the rigid-bodies are visible and time-stamps correspond to the delivered data through the library interface. Being able to acquire such information from several tracked devices reliably, and correctly synchronized, is imperative during CAI. The developments build on top of the Plus Toolkit. Plus is open-source, inherently allows for synchronization between multiple devices and includes support for spatial and temporal calibration information based on the OpenIGTLink protocol. Two new C++ classes were contributed to the toolkit, as well as user documentation.[†] These two classes communicate with the Smart32 API (ConoProbe) and the BiiGOptitrack library (OptiTrack), respectively. Furthermore, the classes were added in such a way that the devices can either be used separately, combined, or together with other devices which are part of the Plus Toolkit. These two contributions enable the Plus application PlusServer to communicate the tracking and measurement information to a client via the OpenIGTLink protocol.

4.4 | 3D Slicer integration

3D Slicer was chosen as the platform for user interactions. 3D Slicer is well documented, can communicate with the OpenIGTLink protocol and inherently allows for intuitive interaction with 3D data (zoom, pan, rotate). It is also extensible through built-in applications, so called modules. Two separate modules have been developed: one for acquiring points with the system and one for reconstructing the surface from the acquired points (or any set of unorganized points).

The ConoProbeConnector module is developed to allow for interaction with the 3D scanning system and its acquired data (Figure 3). The module connects as a client to Plus via OpenIGTLink and allows for point acquisition with the 3D scanning system. The main features of the module are:

- **Real-time 3D visualization:** Points can be recorded and visualized in real time. By setting a principal direction and an interval, the points are coloured in order to make the acquired point-set easier to interpret.
- **Live filtering and post-processing:** By setting a threshold for the signal-to-noise ratio and an interval for the distance (data from the ConoProbe), points can be filtered during acquisition. Once data has been acquired it can also be post-processed with respect to the same parameters.
- **First-person view:** A reference 3D model of the ConoProbe, acquired using an Artec Eva surface scanner (Artec, CA, USA), can be loaded into the module enabling an intuitive first-person view during acquisition.

- **Recording and simulating:** The recorded point-set can be saved both in CSV and VTK format (the CSV-file includes also measurement and tracking information). Additionally, the entire Plus data stream can be recorded and replayed.

The point-set acquired using the ConoProbeConnector module consists of unorganized points. These points provide partial information of an unknown surface. In order to construct a compact representation of this surface, one more module called PointSetProcessing has been developed. The surface reconstruction algorithm in this module works as follows:

- initially, for each point in the point-set, the best fit plane is computed from the set of points within a specified radius of the point. The normal of this plane is then used as an estimate of the normal of the surface that would go through the point. This estimate gives a normal vector at each point in the point-set;
- next, a technique proposed by Hoppe et al[21] is applied to build a nearest neighbour graph on the point-set. An initial orientation is assigned to the normal with the largest z coordinate, and this normal is forced to point in the $+z$ direction. This initial normal direction is then propagated over a minimum spanning tree, computed over the graph;
- finally, a surface is produced from the points and their associated normal vectors using Poisson Reconstruction.[22]

In addition, the module allows for common point-set processing tasks such as smoothing, outlier removal and filtering. The module builds on top of – and improves – existing VTK.[‡] [23,24]
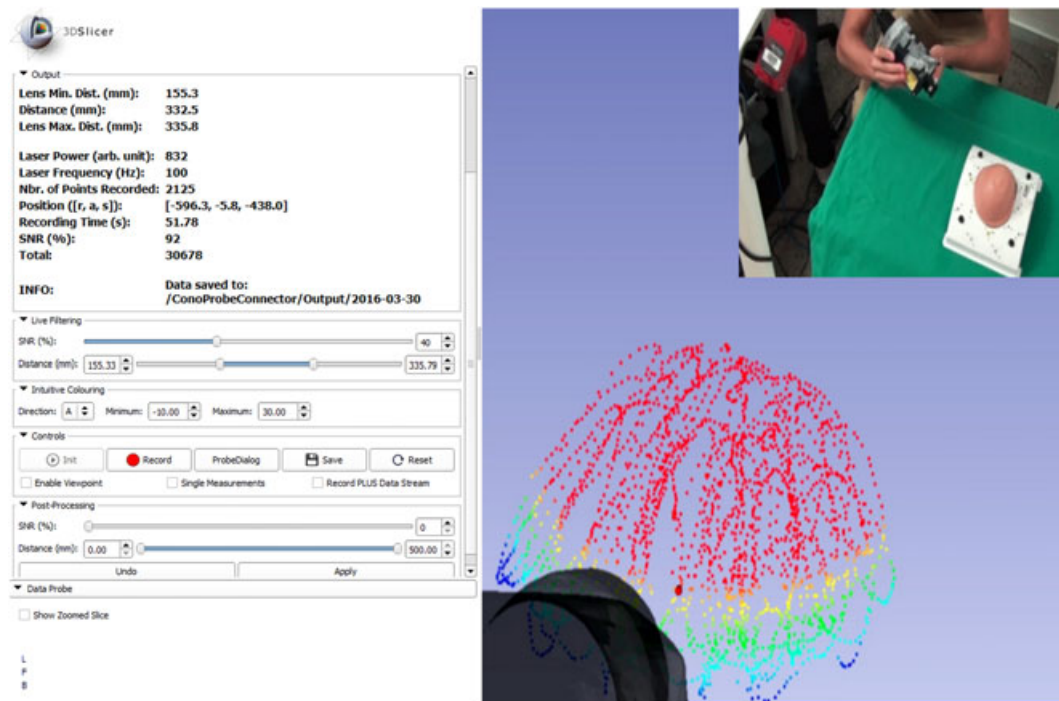
5 | SYSTEM EVALUATION

The evaluation of the 3D scanning system was conducted through a series of experimental tests, using the system components and interfaces previously described. Table 1 summarizes the main characteristics of this evaluation. The computer on which the experiments were carried out was operated with an Intel® Xeon® E3–1271 v3 CPU @ 3.60 GHz processor with 16.0 GB of RAM, Windows 7 SP 1 64-bit, 3D Slicer 4.4.0 and Plus 2.2.0. The five system parameters evaluated were:

- **Update rate:** The update rate of the proposed system (the rate of point acquisition) was measured during all of the experiments. The measurements were acquired on the client side (i.e. in the 3D Slicer module), where the modified event of the OpenIGTLink node was observed. Relevant statistics with respect to both time (ms) and frequency (Hz) were then calculated and summarized.
- **Calibration parameters:** To obtain the time offset (τ), a temporal calibration was performed as previously described: by cross-correlating the first principal component of the rigid body positions with the distance measurements. As for the spatial calibration, in order to estimate the vectors l and $\widehat{d}$, $N = 15$ points at different planes

---

[†]Plus Toolkit: List of devices, http://perk-software.cs.queensu.ca/plus/doc/nightly/user/Devices.html

[‡]The Visualization Toolkit (VTK), http://www.vtk.org/ libraries

FIGURE 3 The ConoProbeConnector module which interfaces with the 3D scanning system (with a photo of the acquisition process superimposed)

TABLE 1 Summary of the ConoSurf scans performed to validate the system

| Validation of	Type	Surface area (cm^2)	No. of points	Acquisition time (s)	Frequency (Hz)	Power (%)	SNR (%)
Point measurement	Calibration TRE	N/A	15	N/A	100	14.7	90
		N/A	15	N/A	100	14.7	90
Surface scan	Multi-step	108.0	20 608	452	100	14.7	90
	Narrow cavity	95.4	30 290	528	100	14.7	90
	Wide cavity	201.2	17 319	387	100	14.7	90
	Breast	174.2	1 523	32	100	15.9	80
Liquid surface scan	Wide cavity	N/A	11 538	381	100	20.3	40

were scanned with the ConoProbe, while recording the distance measurement (d) and the transform **T**. The ConoProbe pose was changed at each point. The GT points were acquired using an optically tracked pointer (Passive 4-marker Probe [Northern Digital Inc., Canada]) by aiming at each point (at the position of the laser spot) with the pointer tip (p'). The vectors l and $\hat{d}$ were determined by least squares fitting of the acquired data.

- **TRE of point measurements:** In order to decide the target registration error (TRE) of the tracked ConoProbe measurements, $N_s = 15$ GT points (p') were acquired using the same optically tracked pointer as in the previous calibration step, and $N_c = 15$ measurement points (p_c) using the tracked ConoProbe system. The average of the Euclidean distance error between these two sets of points was then calculated to obtain the TRE.

- **Surface scanning ability:** ConoSurf's ability to obtain accurate surfaces was assessed by scanning different objects and then registering the acquired, unorganized, point-sets to corresponding GT models. More specifically, four objects were scanned with the ConoSurf system: a multi-step phantom, a narrow and a wide cavity phantom (maximum width × length × depth: 5.8 × 1.8 × 1.9 cm and 7.6 × 7.7 × 2.7 cm, respectively), and a breast phantom (Model 073, CIRS Inc., VA, USA). Figure 4 shows each of the scanned
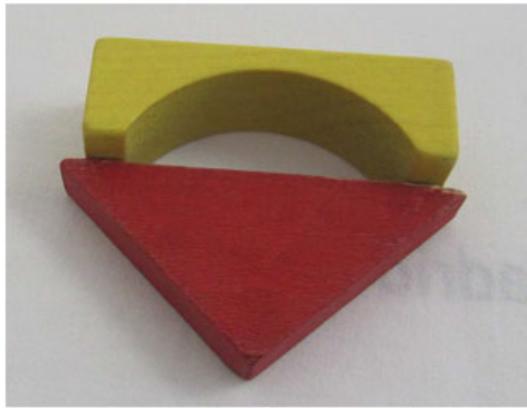
objects. The scans of the multi-step phantom and the cavities were acquired as more time-consuming, high-resolution data; while the breast phantom was a, so called, guidance scan. This guidance scan was defined as a quick, low-resolution scan meant to facilitate guidance during CAI. GT models of the objects were obtained by scanning them in a CT simulator (Toshiba Aquilion LB [Tokyo, Japan]), where all scans had voxel dimensions 0.3 × 0.3 × 0.5 mm. The CT scans were manually segmented using MITK,[§] and the segmentations triangulated using the marching cubes algorithm,[25] in order to obtain the GT data. Each GT model was then rigidly registered to its corresponding point-set acquired with the ConoSurf system using the iterative closest point algorithm,[26] after a manual initialization. The SRE for each point in the acquired model was calculated by finding the corresponding closest point in the GT model of interest and then calculating the Euclidean distance between these two points. Additionally, for the breast phantom, a surface reconstruction was performed using the PointSetProcessing module and the SRE was computed as mentioned above. The surface reconstruction time was measured using a VTK timer.[¶]

[§]The Medical Imaging Interaction Toolkit (MITK), http://mitk.org/

[¶]vtkTimerLog, http://www.vtk.org/doc/nightly/html/classvtkTimerLog.html
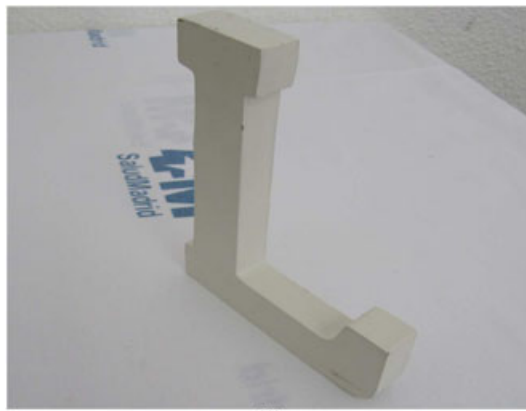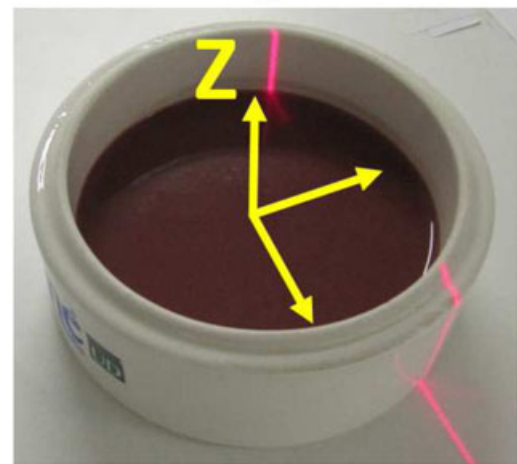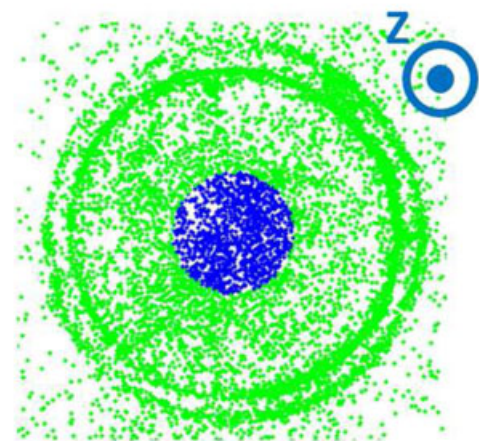
(A)

(B)

(C)

(D)

FIGURE 4 The four objects used in the scanning experiments. Shown are: A, the multi-step phantom; B, the narrow cavity phantom; C, the wide cavity phantom; and D, the breast phantom

(A)

(B)

(C)

FIGURE 5 For the bloody fluid experiment, a container was placed on the table of a CT simulator, with three OptiTrack cameras mounted as in A, and the empty container was scanned with the ConoProbe. Second, a fluid (chicken liver washing) was added to the container B, and one more scan was performed. Next, a GT CT scan was acquired. Finally, a circular region of interest was computed in the CT and the ConoProbe data C, and the difference in fluid height between the GT and the ConoProbe measurements was calculated (Z-direction)

- **Scanning of a liquid surface:** An experiment was carried out in order to assess the system's capability of scanning a surface covered by physiological fluid (Figure 5(A)). First, the wide cavity phantom was scanned with the ConoSurf system. Next, a fluid (chicken liver washing) was added to the phantom (Figure 5(B)), and one more ConoSurf scan was performed. Both ConoSurf acquisitions were performed in the CT room, to avoid displacements or modifications of the scanned object during the experiment. Next, a GT CT scan (Toshiba Aquilion LB), with voxel dimensions 0.3 × 0.3 × 0.5 mm, was performed. Finally, a circular region of interest (ROI) was computed in both the CT (upper and lower region of the fluid) and the ConoProbe data (Figure 5(C)), and the difference in fluid height between the GT and the ConoSurf measurements was calculated (defined as the Z-direction).

6 | RESULTS

The results of the system validation are summarized in four tables. Below are the results corresponding to each evaluated parameter:

- **Update rate:** The mean, standard deviation (SD), and minimum/maximum values of the measured update rate, of the ConoSurf system, is reported in Table 2. The frequency of the point acquisition was computed as 50 Hz.

- **Calibration parameters:** The calibration of the extrinsic and intrinsic parameters of the optical tracking system yielded an overall wand error of 0.240 ± 0.023 mm (mean ± SD). The temporal calibration of the 3D scanning system resulted in a temporal offset of 1 sample (τ = 20 ms), of the optical tracking system relative to the ConoProbe. As for the spatial calibration, the least square fitting resulted in l = [28.59, 60.62, −55.48] mm with a root-mean-square error (RMSE) of 0.98 ± 0.39 mm, and d = [0, 0, −1].

- **TRE of point measurements:** The TRE calculated by comparing the points obtained from tracked pointer with the points from the ConoProbe is shown in Table 3 (mean, Cartesian RMSE, directional RMSEs, SD, maximum). The average TRE for a point measurement was computed as 1.46 mm.

- **Surface scanning ability:** Table 4 shows the calculated SRE (mean, RMSE, SD, maximum) from registering the unorganized point-sets acquired with the 3D scanning system to their corresponding GT-models. Table 5 shows the SREs from registering the unorganized point-set (Figure 6(A)) acquired from the breast phantom, and its

corresponding reconstructed surface, to a GT-model. For better visualization, the result from the surface-to-surface registration can be seen color coded in Figure 6(B). The time taken to reconstruct the breast surface from the point-set was 1.50 s.

- **Scanning of a liquid surface:** As for the bloody fluid experiment; the GT measurements gave a fluid height of 8.1 mm, while the fluid height obtained through the use of the ConoProbe was 8.7 mm. These two values gave a difference between the GT measurements and the ConoProbe of 0.6 mm.

7 | DISCUSSION

In this work we have made available to the CAI community ConoSurf, an open-source software system for acquiring surface data using a tracked conoscopic holography device (available at http://hggm-lim.github.io/ConoSurf/). The system has been validated on a liquid surface as well as on several complex shaped phantoms, which included sharp edges, corners, holes, etc. In addition, by performing a guidance scan on a breast phantom, it has been shown that the system can be used to acquire a smooth approximation of a surface which could be useful during image-guided scenarios.

The scanning system is integrated into the Plus Toolkit and is therefore extensible to not only using a multi-camera tracking system, but also many other types of tracking systems supported by Plus. All these developments are integrated into 3D Slicer, facilitating a quick adoption as well as future enhancements. The PointSetProcessing module introduces features currently not available in 3D Slicer and could be applied to any application where a robust surface reconstruction is necessary. This surface data could allow calculating an updated dose-distribution during IOERT procedures without the use of additional intraoperative CT imaging. Furthermore, as intraoperative information nowadays is important during CAI, preoperative images could be updated with the intraoperative data (surface) acquired by the ConoProbe. Gombos et al[27] have recently described their experience with a supine intraoperative MR imaging protocol to evaluate tumor deformation. For the same procedure, Ungi et al[28] propose an US-based framework relying on a tracked stylus for acquiring the necessary surface points. In such scenarios, the ConoProbe could acquire surface data or point positions without touching the patient. This information would not be as complete as a 3D MR volume, but could be a simple method easily available thanks to this open-source contribution.

TABLE 2 Statistics related to the update rate of the 3D scanning system

	Mean (Hz)	Mean (ms)	SD (ms)	Min (ms)	Max (ms)
Update rate	50.3	20	4	10	35

TABLE 3 Experimentally determined target registration error (TRE) for a point measurement. All values are in mm

	Mean	RMSE$_{\|.\|}$	RMSE$_x$	RMSE$_y$	RMSE$_z$	SD	Max
Point measurement	1.46	1.56	0.65	1.00	1.01	0.56	2.67

TABLE 4 SREs from registering the high-resolution point-sets to GT-models. All values are in mm

Registration	Object	Mean	RMSE	SD	Max
Point-set to GT	Multi-step	1.18	1.35	0.65	4.91
	Narrow cavity	1.10	1.23	0.56	3.71
	Wide cavity	1.29	1.51	0.87	7.43
	Total (mean)	1.19	1.36	0.69	5.35

TABLE 5 SREs from registering the point-set acquired from the breast phantom, and its corresponding reconstructed surface, to a GT-model. All values are in mm

Registration	Mean	RMSE	SD	Max
Point-set to GT	1.68	2.31	1.52	5.86
Surface to GT	1.30	1.83	1.24	5.17
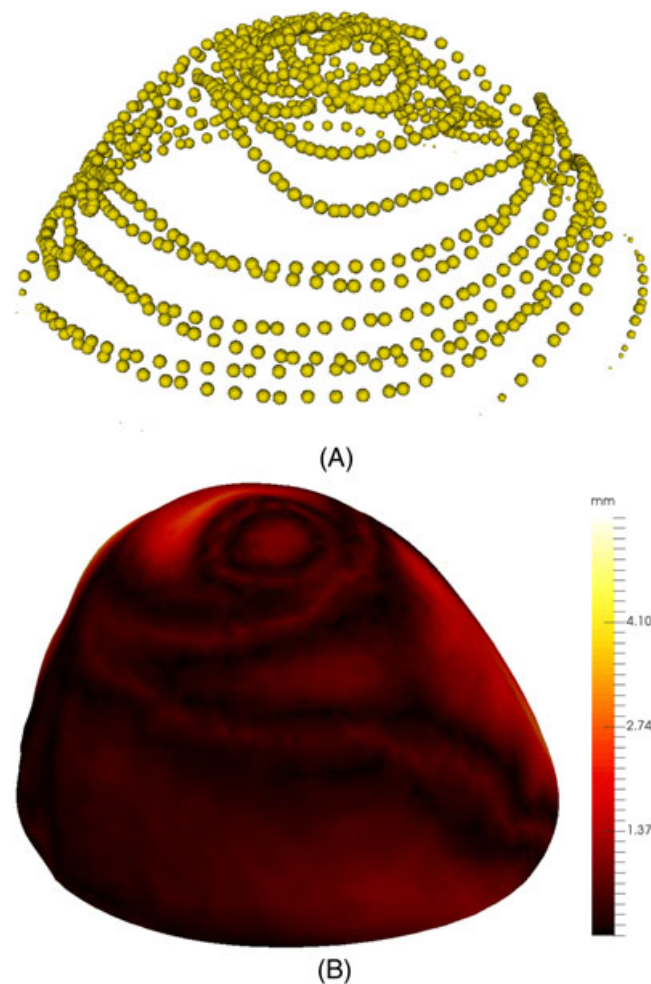
FIGURE 6 Example of point-set acquired from the breast phantom and the corresponding surface reconstruction. A, The point-set acquired with the ConoSurf system. B, Registration result between the GT model and the reconstructed breast surface, in the form of the SRE, colour coded with unit in mm

The fast guidance scan performed on a breast phantom (acquisition time just above 30 s), followed by a quick surface reconstruction of the acquired unorganized point-set (1.50 s) showed a mean SRE of 1.30 mm. The results in Table 5 show that the SRE for a guidance scan is larger when compared with the results of the high-resolution scans in Table 4. This result was expected because the number of points in the breast phantom acquisition was much smaller. More noteworthy is that the SRE for the breast phantom decreases for the reconstructed surface (1.30 mm) compared with the point-set (1.68 mm). This result verifies our choice of surface reconstruction technique as a solution to improve robustness and accuracy when a very low number of surface points have been acquired. The proposed technique could therefore prove valuable in CAI applications where surface data is reconstructed from point data. Besides Poisson reconstruction, we also experimented with Delaunay triangulation but failed to produce adequate results.

A TRE of 1.56 mm (RMSE) for point measurements is larger than the value (0.77 mm) Burgner et al reported in an earlier study,[17] in which they used the same conoscopic holography device to scan a human cadaver kidney. Their lower TRE is most likely due to their optical tracking system (Polaris Spectra [Northern Digital Inc., Canada]) and their lower spatial calibration error (0.58 mm compared with our 0.98 mm). When comparing results of point-set registrations (Table 4), ConoSurf's mean error of 1.19 mm is close to the 1.13 mm (average of kidney phantom and *ex vivo* kidney mean TRE) reported in the earlier study. This similar value, in the presence of a larger spatial calibration error, could be a result of the real-time visualization, which is helpful for filling in sparse regions of the acquired point-set, consequently leading to more precise registrations. When comparing ConoSurf's point-set registration results with those from studies in which they used a single-shot device (such as time-of-flight cameras or structured light scanners) we find that their registration errors are in the same range as ours.[29,30]

A scanning experiment was also carried out on a bloody fluid obtaining a mean measurement difference of 0.6 mm when compared with the same object without fluid. This result leads us to conclude that the conoscopic holography is a good candidate for acquiring surfaces intraoperatively where regions of fluid can accumulate. This paper is the first one to present results of this device on fluids.

A limitation of the presented system is that the ConoProbe is a single-point measurement device. Compared with single-shot devices the system presented in this paper needs to be aimed at, and moved along, the desired surface in a point-wise manner. This need for translation of the acquisition point makes it more sensitive to patient movements and also increases the acquisition time. Our 3D scanning system currently acquires points with a frequency of 50 Hz, which is far from the maximum frequency of the ConoProbe itself (9 kHz); therefore, by increasing the system update rate, surfaces are bound to be acquired in less time. Finally, our high-resolution scanning experiments were acquired from three phantoms of complex shape (which included sharp corners, narrow hollows and fine protrusions). The complexity of the phantoms increased acquisition time, since the ConoProbe laser-spot had to cover a large working area, but were of interest because of the difficulty they presented to the scanning procedure. For smoother surfaces, like organs, we expect the acquisition time to be substantially less with decreased SRE as well.

Future work will focus on increasing update rate, improving spatial calibration approach and including these calibration methods in the 3D Slicer module. We will also test these developments on preclinical and clinical data in order to improve dose estimation on IOERT procedures.

ACKNOWLEDGMENTS

CONFLICT OF INTEREST

The authors declare that they have no conflict of interest.

FUNDING

REFERENCES

1. Markelj P, Tomaževič D, Likar B, et al. A review of 3D/2D registration methods for image-guided interventions. *Med Image Anal*. 2012;16(3):642–661.

2. Peters T, Cleary K. *Image-Guided Interventions: Technology and Applications*. New York, USA: Springer Science & Business Media; 2008.

3. Dogangil G, Davies BL, Rodriguez y Baena F. A review of medical robotics for minimally invasive soft tissue surgery. *Proc IME H J Eng Med*. 2010;224(5):653–679.

4. Senft C, Bink A, Franz K, et al. Intraoperative MRI guidance and extent of resection in glioma surgery: a randomised, controlled trial. *Lancet Oncol*. 2011;12(11):997–1003.

5. Rafferty MA, Siewerdsen JH, Chan Y, et al. Intraoperative cone-beam CT for guidance of temporal bone surgery. *Otolaryngol Head Neck Surg*. 2006;134(5):801–808.

6. Brudfors M, Seitel A, Rasoulian A, et al. Towards real-time, tracker-less 3D ultrasound guidance for spine anaesthesia. *Int J Comput Assist Radiol Surg*. 2015;10(6):855–865.

7. Schicho K, Figl M, Seemann R, et al. Comparison of laser surface scanning and fiducial marker-based registration in frameless stereotaxy: technical note. *J Neurosurg*. 2007;106(4):704–709.

8. Cash DM, Sinha TK, Chapman WC, et al. Incorporation of a laser range scanner into image-guided liver surgery: surface acquisition, registration, and tracking. *Med Phys*. 2003;30(7):1671–1682.

9. Simpson AL, Burgner J, Glisson CL, et al. Comparison study of intraoperative surface acquisition methods for surgical navigation. *IEEE Trans Biomed Eng*. 2013;60(4):1090–1099.

10. Lathrop R, Hackworth DM, Webster RJ. Minimally invasive holographic surface scanning for soft-tissue image registration. *IEEE Trans Biomed Eng*. 2010;57(6):1497–1506.

11. Simpson AL, Sun K, Pheiffer TS, et al. Evaluation of conoscopic holography for estimating tumor resection cavities in model-based image-guided neurosurgery. *IEEE Trans Biomed Eng*. 2014;61(6):1833–1843.

12. Pascau J, Santos-Miranda J, San-Segundo CG, et al. Intraoperative imaging in IOERT sarcoma treatment: initial experience in two clinical cases. *Int J Radiat Oncol Biol Phys*. 2011;81(2):S90

13. Consorti R, Petrucci A, Fortunato F, et al. *In vivo* dosimetry with MOSFETs: dosimetric characterization and first clinical results in intra-operative radiotherapy. *Int J Radiat Oncol Biol Phys*. 2005;63(3):952–960.

14. Costa F, Sarmento S, Sousa O. PD-0574: dose distributions in pelvic intraoperative radiation therapy (IOERT). *Radiother Oncol*. 2015;115:280–281.

15. Fedorov A, Beichel R, Kalpathy-Cramer J, et al. 3D slicer as an image computing platform for the quantitative imaging network. *Magn Reson Imag*. 2012;30(9):1323–1341.

16. Lasso A, Heffter T, Rankin A, et al. PLUS: open-source toolkit for ultrasound-guided intervention systems. *IEEE Trans Biomed Eng*. 2014;61(10):2527–2537.

17. Burgner J, Simpson AL, Fitzpatrick JM, et al. A study on the theoretical and practical accuracy of conoscopic holography-based surface measurements: toward image registration in minimally invasive surgery. *Int J Comput Assist Radiol Surg*. 2013;9(2):190–203.

18. García-Vázquez V, Marinetto E, Santos-Miranda JA, et al. Feasibility of integrating a multi-camera optical tracking system in intra-operative electron radiation therapy scenarios. *Phys Med Biol*. 2013;58(24):8769

19. Treece GM, Gee AH, Prager RW, et al. High-definition freehand 3-D ultrasound. *Ultrasound Med Biol*. 2003;29(4):529–546.

20. Tokuda J, Fischer GS, Papademetris X, et al. OpenIGTLink: an open network protocol for image-guided therapy environment. *Int J Med Robot*. 2009;5(4):423–434.

21. Hoppe H, DeRose T, Duchamp T, *et al*. Surface reconstruction from unorganized points. In *Proceedings of the 19th annual conference on Computer graphics and interactive techniques, ser. SIGGRAPH '92*. ACM: New York, USA; 1992;71–78.

22. Kazhdan M, Bolitho M, Hoppe H. Poisson surface reconstruction. In *Proceedings of the 4th Eurographics symposium on Geometry processing, ser. SGP '06*. Eurographics Association: Aire-la-Ville, CH; 2006;61–70.

23. Doria D, Gelas A. Poisson surface reconstruction for VTK. *The VTK Journal* [Internet]. 2010 Mar [cited 2015 Aug 15]. Available from: http://hdl.handle.net/10380/3155

24. Doria D. Point set processing for VTK – outlier removal, curvature estimation, normal estimation, normal orientation. *The VTK Journal* [Internet]. 2011 Aug [cited 2015 Aug 15]. Available from: http://hdl.handle.net/10380/3143

25. Lorensen WE, Cline HE. Marching cubes: a high resolution 3D surface construction algorithm. In *Proceedings of the 14th annual conference on Computer graphics and interactive techniques, ser. SIGGRAPH '87*. ACM: New York, USA;1987; 163–169.

26. Besl PJ, McKay ND. Method for registration of 3D shapes. *IEEE Trans Pattern Anal Mach Intell*. 1992;14(2):239–254.

27. Gombos EC, Jayender J, Richman DM, et al. Intraoperative supine breast MR imaging to quantify tumor deformation and detection of residual breast cancer: preliminary results. *Radiology*. 2016;151472 Epub 2016 Jun 22.

28. Ungi T, Gauvin B, Lasso A, et al. Navigated breast tumor excision using electromagnetically tracked ultrasound and surgical instruments. *IEEE Trans Biomed Eng*. 2016;63(3):600–606.

29. Maier-Hein L, Groch A, Bartoli A, et al. Comparative validation of singleshot optical techniques for laparoscopic 3-D surface reconstruction. *IEEE Trans Med Imaging*. 2014;33(10):1913–1930.

30. Lacher RM, Hipwell JH, Williams NR, Keshtgar MR, Hawkes DJ, Stoyanov D. Low-cost surface reconstruction for aesthetic results assessment and prediction in breast cancer surgery. In *Proceedings of the 37th Annual International Conference of the IEEE Engineering in Medicine and Biology Society, ser. EMBC '15*. IEEE: New York, USA; 2015; 5871–5874.